Mechanisms for plasma and reactive ion etch-front roughening

Jason T. Drotar, Y.-P. Zhao, T.-M. Lu, and G.-C. Wang
Department of Physics, Applied Physics, and Astronomy, Rensselaer Polytechnic Institute, Troy, New York 12180-3590
(Received 14 April 1999; revised manuscript received 1 September 1999)

Through extensive $(2+1)$-dimensional numerical integration and Monte Carlo simulations, we compute the scaling exponents of a flux redistribution model that is proposed to describe plasma etching and reactive ion etching of surfaces. It is found that, while the surface morphology depends on the etching conditions, the roughness exponent α, the growth exponent β, and the dynamic exponent z are universal with regard to the details of the re-emission mechanism and are given by $\alpha \approx \beta \approx z \approx 1$. These exponents are in agreement with recent experiments on plasma etch-front roughening.

I. INTRODUCTION

Growth and etching of thin films are key processing techniques of many high-technology industries. It is well known that, under nonequilibrium conditions, growth/etch fronts can exhibit different degrees of roughness, depending on processing conditions such as temperature, pressure, and rate of growth or etching. Most of the work to date has focused on the study of growth front roughening phenomena in physical vapor condensation (PVC) [including sputtering, molecular beam epitaxy (MBE), etc].[1,2] Although plasma etching is a key technique in modern microelectronics fabrication, so far most work has focused on the evolution of trenches.[3–5] Few works have been reported on the dynamic roughening of plasma etch fronts. Recently, Brault, Dumas, and Salvan showed that the interface width w induced by SF_6 plasma etching of silicon surfaces increases linearly with etch time ($w \sim t^1$) and that the lateral correlation length ξ grows as a power law, $\xi \sim t^{0.66}$.[6] They attributed this behavior to the shadowing effect, which has been used to describe sputtering growth.[7]

The basic idea of the shadowing effect in sputtering growth is that the crest of the surface will receive more deposited atoms than the valley of the surface because the receiving solid angle at the crest is larger than that in the valley. Therefore the growth rate at the peak is faster than that in the valley, which causes a growth instability. However, if one applies this model to plasma etching, suggesting that peaks have a faster etching rate than valleys, one would expect stable growth with a growth exponent $\beta < 0.5$. Thus, it appears that shadowing effects cannot account for the instability observed in plasma etching. Recently, we also studied the scaling behavior of plasma-etched Si(100) interfaces and found that $\alpha = 0.96$, $\beta = 0.91$, and $z = 1.05$.[8] This behavior is not consistent with any of the known universality classes. Furthermore, the fact that $\beta > 0.5$ implies that some other roughening mechanism besides noise is present.

Plasma etching has at least three different modes: conventional plasma etching (neutral chemical reaction only), reactive ion etching (RIE), and high-density plasma etching. In the plasma-etching mode, the electrons accelerated by the applied rf field in the plasma sheath collide with gas atoms and molecules. Some atoms and molecules are dissociated or ionized to form radicals, atoms, and ions during the collisions. The active species (radicals, ions, etc.) are then transported to the sample surface where they are adsorbed and react with, or desorb from, the sample. The etching products are volatile and desorb from the sample. Usually, for plasma etching, the gas pressure is 100–300 mTorr, and the sample is grounded during etching. The main etching mechanism, in this case, is radical chemical etching. This is the case in our experiment.[8] For RIE, the gas pressure is less than 100 mTorr, and the sample is floating or biased. In this case, both chemical etching by radicals and physical bombardment by ions contribute to the etching. Ion-enhanced etching is the case for Ref. 6. For high-density plasma etching, such as inductively coupled plasma systems,[9] the ratio of the ion flux to the reactive neutral flux is larger. Even in this case, the physical sputtering effect is small and can be neglected. There are two extremes: conventional plasma etching, for which the etching rate of ions can be neglected, and high-density plasma etching, for which ion etching is dominant.

For plasma etching, the gas flux can come from all directions (unless the substrate is strongly biased), and the gas atoms have a broad energy distribution and angular distribution of momentum. The etching dynamics are governed mainly by the dynamics of the gas transport process as demonstrated by trench evolution during plasma etching.[3–5] Two very important features, microtrenching and undercutting, usually occur during trench etching. Microtrenching means that the etching rate is higher near the corners of a trench compared to the center of the trench, and therefore a microgroove is formed at the corners. It has been shown that the reflection of grazing incidence ions from the sidewall of a trench can cause microtrenching.[3] This process redistributes the flux of ions at the bottom of the features, and flux peaks away from the sidewall.[3] Undercutting means that the sidewall of a trench under the mask can be etched away. It can be modeled using the concept of thermal reemission from the surface.[4] Singh, Shaqfeh, and McVittie argue that reactants incident on the substrate with thermal velocity might be reemitted from the surface before they react.[5] The reemitted flux has a cosine distribution with respect to the surface normal. Thus the sidewall may receive more reactants than other places.

Recently, using the molecular beam method, Hwang *et al.* performed a detailed study of the scattering of energetic F atoms on a fluorinated Si surface.[10] They showed that the redistribution of the F-atom flux is due to three distinct scattering processes: directly inelastic scattering (DIS) is respon-

sible for microtrench formation, while both indirectly inelastic scattering (IIS) and trapping desorption (TD) (i.e., reemission) are responsible for undercutting. The flux redistribution process depends on the local environment around the studied position. Therefore, one would expect very different roughening dynamics for plasma etching compared to PVC.

In the present work, we extend the deterministic reemission model proposed by Singh, Shaqfeh, and McVittie,[5] which was used to describe trench evolution during plasma etching, to include noise. The noise is responsible for initiating etch-front roughening, and the extended model can explain the scaling exponents that were obtained experimentally by us[8] and the growth exponent that was obtained experimentally by Brault, Dumas, and Salvan.[6] We demonstrate the behavior of this model using both numerical integration and a Monte Carlo simulation and compare the results to existing universality classes and experimental systems.

II. PLASMA ETCHING AND REACTIVE ION ETCHING MODELS

The model we studied is based on the idea of flux reemission as presented in Ref. 5. Since the pressure in a typical plasma-etching system is on the order of 100 mTorr, the Knudsen number (the ratio of the mean free path of any gas particles to the characteristic length of the surface features) is large. Hence, collisions between particles within surface features can be neglected. Therefore, the etching particles can travel in a straight line until hitting the surface at another point. We also assume that the surface evolves slowly compared to the redistribution of flux due to the surface features. In this model, particles are incident on a surface, and a given particle either etches the surface at the point of incidence or is reemitted in a direction that depends on the reemission mode. The probability of an incoming particle sticking to the surface is s_0 $(0 \leqslant s_0 \leqslant 1)$, where s_0 is called the zeroth-order sticking coefficient. Incoming particles are called zeroth-order particles, while an nth-order particle that has been reemitted is called an $(n+1)$th-order particle. The probability of an nth-order particle sticking is s_n $(0 \leqslant s_n \leqslant 1)$, and there is a probability of $1-s_n$ that this particle will not stick, but will, instead, go somewhere else (in other words, the flux is redistributed).

The model assumes a two-dimensional surface described by a height function $h(\mathbf{r},t)$, where $\mathbf{r}=(x,y)$. Implicit in this sort of description is the absence of overhangs. We denote the overall flux of nth-order particles at in-plane position $\mathbf{r}$ at time t by $F_n(\mathbf{r},t)$. The surface evolution can be described by the continuum equation

$$\frac{\partial h}{\partial t} = \nu\nabla^2 h - \kappa\nabla^4 h \mp \sqrt{1+(\nabla h)^2} \times [s_0 F_0(\mathbf{r},t) + s_1 F_1(\mathbf{r},t) + \cdots] + \eta, \tag{1}$$

where the condensation/evaporation term $\nu\nabla^2 h$, the surface diffusion term $-\kappa\nabla^4 h$, and the noise term η have been added in. The inherent noise in the etching or growth process satisfies

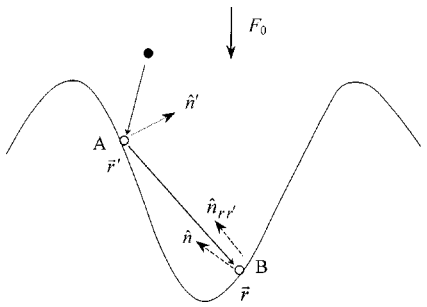

FIG. 1. Flux reemission: the incoming particle can be reemitted from point *A* to land at point *B*.

$$\langle \eta(\mathbf{r},t) \rangle = 0 \tag{2}$$

and

$$\langle \eta(\mathbf{r},t)\,\eta(\mathbf{r}',t') \rangle = 2D\,\delta(\mathbf{r}-\mathbf{r}')\,\delta(t-t'). \tag{3}$$

The minus sign in front of the third term in Eq. (1) indicates an etching process and the plus sign indicates deposition. Also, we have taken into account that the growth or etching takes place in the direction normal to the surface by putting a factor of $\sqrt{1+(\nabla h)^2}$ in front of the flux terms. The main difficulty lies in finding each F_n. Following the reasoning in Ref. 5, the F_n satisfy, for diffuse reemission (which we will define later),

$$F_{n+1}(\mathbf{r},t) = (1-s_n) \int Z(\mathbf{r},\mathbf{r}',t) F_n(r',t) \times \frac{(\hat{\mathbf{n}}_{\mathbf{rr}'} \cdot \hat{\mathbf{n}}) P(\hat{\mathbf{n}}_{\mathbf{r}'\mathbf{r}}, \hat{\mathbf{n}}')}{(\mathbf{r}-\mathbf{r}')^2 + (h-h')^2} dA', \tag{4}$$

where $\hat{\mathbf{n}}$ is the unit normal pointing out of the surface at position $\mathbf{r}$, $\hat{\mathbf{n}}'$ is the unit normal at position $\mathbf{r}'$, $\hat{\mathbf{n}}_{\mathbf{rr}'}$ is the unit vector pointing from $\mathbf{r}$ to $\mathbf{r}'$, and $\hat{\mathbf{n}}_{\mathbf{r}'\mathbf{r}}$ is the unit vector pointing from $\mathbf{r}'$ to $\mathbf{r}$. $P(\hat{\mathbf{n}}_{\mathbf{r}'\mathbf{r}}, \hat{\mathbf{n}}')$ is the probability distribution of the reemitted flux (the probability per solid angle that the particle will be reemitted in the given direction) and, for thermal reemission (as we will see later),[4] is equal to $(\hat{\mathbf{n}}_{\mathbf{r}'\mathbf{r}} \cdot \mathbf{n}')/\pi$. $Z(\mathbf{r},\mathbf{r}',t)$ is equal to 1 except when there is no line of sight between the surface elements at $\mathbf{r}$ and $\mathbf{r}'$ or $(\hat{\mathbf{n}}_{\mathbf{rr}'} \cdot \mathbf{n})$ is negative, in which case Z is zero. The reemission model is illustrated in Fig. 1.

The model that we have so far described has many unknowns left in it:

(1) *The characteristics of* F_0. As we have discussed in the Introduction, in plasma etching, both chemical etching by radicals and physical bombardment by ions can occur. For chemical etching, radicals can come from all directions (no directionality), i.e., the incoming radicals have a broad angular distribution. However, for ion-assisted etching, the ions are directed more perpendicularly to the sample surface. Therefore, in the present work, we consider only two possibilities for F_0: incoming particles can come either from all directions (no directionality), or from one given direction (perfect directionality). Intermediate cases or combinations of these two can exist in RIE processes, but we consider only these two extremes. For particles coming from all directions, the shadowing effect of the surface features on the incoming flux cannot be ignored, and one must take into account the surrounding surface when computing the incoming flux (F_0)

for a point on the surface. In this case, F_0 is simply the value obtained by considering the shadowing effect. Since shadowing has been studied extensively,[7] we do not discuss it here. When considering particles incident from a given direction, we consider only normal incidence. For normal incidence, there is no shadowing effect, and F_0 is equal to $1/\sqrt{1+(\nabla h)^2}$. However, as we shall see later, the exact form of F_0 has little effect on the main behavior of our model.

(2) *The mode of reemission*. It is necessary to specify exactly what happens to particles that do not stick. For example, in what direction do they go off? Does this depend on the direction from which the particle came? The redistribution of the incoming flux is the result of the gas-solid interactions.[11–13] The solid surface imposes a boundary, which affects the behavior of the gas transport. Therefore the redistribution strongly depends on surface conditions such as roughness, physical or chemical adsorption, and surface chemical reaction. In general, there are two simplified reemission modes: thermal and specular reemission. Thermal reemission means that all the incoming particles reach thermal equilibrium with the surface instantly and then are reemitted from the surface to the gaseous state with a Maxwellian distribution of velocities that depends on the surface temperature. The transition probability, $R(\mathbf{v}'\rightarrow\mathbf{v})$, which represents the probability of an incoming particle with velocity $\mathbf{v}'$ being reemitted back into the gas with velocity $\mathbf{v}$, is

$$R(\mathbf{v}'\rightarrow\mathbf{v})=\mathbf{v}\cdot\hat{\mathbf{n}}\frac{1}{2\pi\theta_s^2}\exp\left(-\frac{v^2}{2\theta_s}\right).$$

Here, $\theta_s=k_BT_s/m$, k_B is the Boltzmann constant, T_s is the surface temperature, and m is the particle mass. The probability per solid angle of the redistributed flux has the form $P=(\hat{\mathbf{n}}_{\mathbf{r}'\mathbf{r}}\cdot\hat{\mathbf{n}}')/\pi$. The reemission, in this case, is diffuse. In other words, a reemitted particle carries no knowledge of its prior velocity.

Specular reflection assumes that when an incoming particle with velocity $\mathbf{v}'$ hits the surface, it reflects into the gas with velocity $\mathbf{v}=\mathbf{v}'-2\hat{\mathbf{n}}(\hat{\mathbf{n}}\cdot\mathbf{v}')$. The transition probability becomes $R(\mathbf{v}'\rightarrow\mathbf{v})=\delta(\mathbf{v}-\mathbf{v}'+2\hat{\mathbf{n}}(\hat{\mathbf{n}}\cdot\mathbf{v}'))$. The probability of the redistributed flux is $P=1$ at the reflected direction and $P=0$ at other directions. These two modes are ideal cases that may not apply to realistic cases. In order to be more realistic, Maxwell assumed that the transition probability is between these two ideal cases,

$$R(\mathbf{v}'\rightarrow\mathbf{v})=(1-\chi)\,\delta(\mathbf{v}-\mathbf{v}'+2\hat{\mathbf{n}}(\hat{\mathbf{n}}\cdot\mathbf{v}'))+\chi\mathbf{v}\cdot\hat{\mathbf{n}}\frac{1}{2\pi\theta_s^2}\exp\left(-\frac{v^2}{2\theta_s}\right).$$

Here $0\leqslant\chi\leqslant1$ is called the accommodation coefficient, which depends on the energies of the incoming particles and reemitted particles, and the surface temperature.[11–13] In this case, since particles come from all directions, we simply assume that the probability distribution of the redistributed flux is a constant, $P=1/2\pi$, and we call this uniform redistribution. However, the real situation could be even more complicated than what we have discussed above, as in the experiment of Hwang *et al.*[10] These reemission modes are illustrated in Fig. 2.

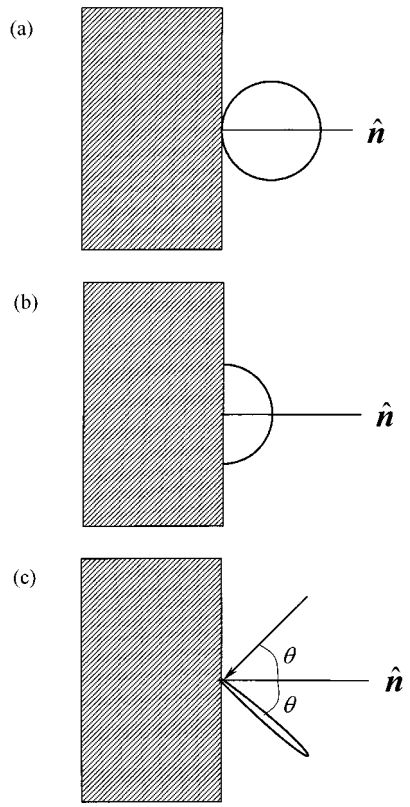

FIG. 2. Polar plots of flux distributions for (a) thermal reemission, (b) uniform reemission, and (c) specular reemission.

(3) *The value of the nth-order sticking coefficient s_n for each n*. For simplicity, we consider only etching with $s_0\approx0$ and $s_1=1$. If we let, for some n, $s_n=1$ and $s_j\approx0$ for $j<n$, then we have an nth-order reemission process. An example of zeroth-order reemission ($s_0=1$) is shadowing, which has already been studied for the case of growth.[7] Our case corresponds to first-order reemission etching.

It is possible to describe the surface evolution of our model quantitatively. From the calculated surfaces, one can compute the time dependent height-height correlation function,

$$H(\mathbf{r},t)=\langle[h(\mathbf{r}+\mathbf{r}',t)-h(\mathbf{r}',t)]^2\rangle, \tag{5}$$

from which important statistical information about the surfaces can be obtained. The averaging is done over the $\mathbf{r}'$ variable. We assume that the height-height correlation function has the form[14]

$$H(\mathbf{r},t)=2[w(t)]^2f\left(\frac{r}{\xi(t)}\right), \tag{6}$$

with $f(r)\propto r^{2\alpha}$ for $r\ll1$ and $f(r)=1$ for $r\gg1$. Here $w(t)$ is the interface width defined by $w(t)^2=\langle[h(\mathbf{r},t)-\overline{h}(t)]^2\rangle$, where $\overline{h}(t)$ is the average height of the surface and the average is over all $\mathbf{r}$, $\xi(t)$ is the lateral correlation length, and α is called the roughness exponent. These parameters are assumed to characterize the individual surfaces completely. However, one can also characterize the dynamic behavior of the model by looking at how these parameters evolve with time. We assume that both $w(t)$ and $\xi(t)$ evolve in time as power laws,

$$w \propto t^{\beta}, \tag{7}$$

and

$$\xi \propto t^{1/z}, \tag{8}$$

where β and z are the growth and dynamic exponents, respectively. The parameters α, β, and z are not independent, but are assumed to satisfy

$$z = \alpha/\beta. \tag{9}$$

Since the surfaces generated by our model consist of holes, one can also look at the evolution of the average hole separation distance λ. We assume that

$$\lambda \propto t^{\gamma}. \tag{10}$$

It is possible to solve Eq. (1) by numerical integration. This was done on a 128×128 periodic lattice with $\nu = 0.5$, $\kappa = 0$, $s_0 = 0.05$, and $s_1 = 1$. The redistribution was thermal, and the noise was turned off after a short period after which the system evolved deterministically (for this sort of etching, though, the noise should only be important in the early stages of surface evolution). Also, the flux at each point was computed considering only points within a 65×65 square centered on the point; this square must be significantly larger than the correlation length ξ for the simulation to be accurate. The incoming flux was nondirectional, and for unshadowed points, we let $F_0 = 4$ (F_0 was, of course, less for shadowed points). The parameter values were chosen such that the asymptotic behavior of the reemission term could be easily seen. However, if we had set $\nu = \kappa = 0$, singularities would have developed in the solution. Such solutions, though, are not physically realistic and exist only because our model assumes an absence of overhangs. The $\nabla^2 h$ term, if sufficiently large, eliminates this problem, but obscures the scaling behavior of the reemission term. It therefore should be only large enough to stabilize the equation. The F_0 term determines the time scale of the morphology evolution. The last consideration is the noise. Noise is necessary to start the roughening process, but should not be so large that it obscures the effect of the reemission term. In Fig. 3, we show the calculated surface images for different times. The surfaces consist of holes. These holes coalesce and become larger with increasing etch time, even for later times. The interface width versus time, as shown in Fig. 4, has a linear dependence, which is consistent with $\beta = 1$. The height-height correlation functions show a roughness exponent of $\alpha = 0.98$. We saw a similar behavior for the case of thermal reemission with directional flux.

Equation (1) explicitly demonstrates how flux redistribution affects the etching morphology. However, the redistributed flux at certain surface points depends on the surrounding environment as illustrated by the integral equation, Eq. (4). Numerical integration has some serious drawbacks when applied to the model we are studying. The biggest drawback is the computation time required for large system sizes. This limitation makes it difficult to run simulations larger than 128×128 on a desktop computer. Also, one must carefully consider the issue of stability. Of course, Δt must be made small enough to ensure numerical stability, but even if this requirement is met, singularities can still develop in the solutions. One reason for this type of occurrence is that our model assumes the absence of overhangs. If the model is such that overhangs actually can occur, then the equation describing h should actually predict singularities. In our case we avoid singularities by including a $\nabla^2 h$ term. The final drawback is the need to turn the noise off after a short time. The noise produces an early-time scaling regime that obscures the scaling behavior of the reemission term. Of course, there should eventually be a crossover to linear behavior, but if the noise is left on, the crossover time is very long.

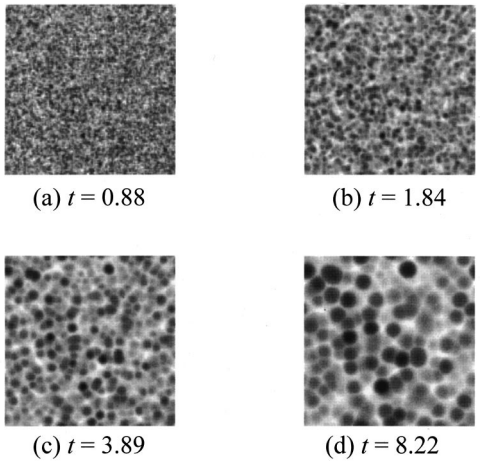

FIG. 3. Calculated surfaces for various times with a 128×128 lattice, $\nu = 0.5$, $\kappa = 0$, $s_0 = 0.05$, $s_1 = 1$, and $F_0 = 4$. (a) $t = 0.88$, (b) $t = 1.84$, (c) $t = 3.89$, and (d) $t = 8.22$. The gray scale is adjusted so that the highest point on the surface is white and the lowest point on the surface is black.

III. MONTE CARLO SIMULATIONS

In order to determine more efficiently how different redistribution models affect the morphological evolution of the surface, a Monte Carlo simulation can be employed. The method is illustrated in Fig. 5. A periodic $N \times N$ lattice is still used, but the height h is allowed to take on only integer values. The simulation proceeds according to a simple set of

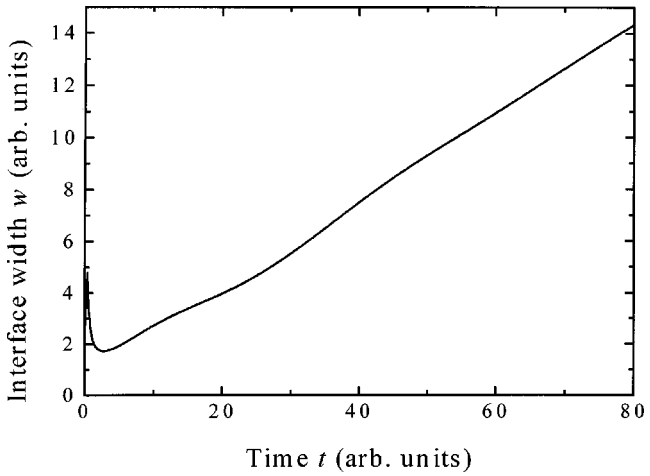

FIG. 4. Interface width w vs time for calculated surfaces with a 128×128 lattice, $\nu = 0.5$, $\kappa = 0$, $s_0 = 0.05$, $s_1 = 1$, and $F_0 = 4$.

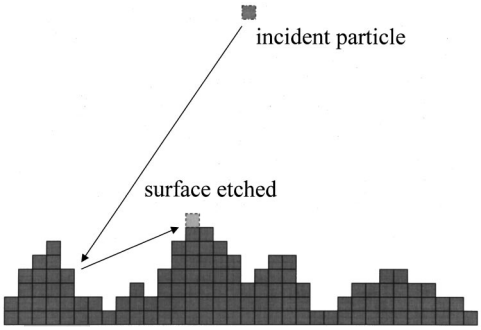

FIG. 5. The Monte Carlo simulation of the redistribution model: An incoming particle bounces off the surface and then etches the surface elsewhere.

rules. A single particle (with a position described by x, y, and z) is introduced with a random (uniformly distributed) x and y, and z is set to the maximum height of the surface, plus one. For the case of no directionality in F_0, the direction of the particle follows the distribution $dP(\theta,\phi)/d\Omega = (\cos\theta)/\pi$, where ϕ is the angle of the projection of the particle's trajectory in the xy plane, θ is the angle between the particle's trajectory and the z axis, and $d\Omega$ is equal to $d(\cos\theta)d\phi$. For the case of perfect directionality, θ is a constant ($\theta=0$ for normal incidence), and ϕ is uniformly distributed between 0 and 2π. The particle moves in a straight line until it hits the surface and either etches the surface (or is deposited, in the case of growth) or is reemitted according to the details of the reemission mode. The particle then travels in a straight line until it hits the surface again or heads away from the surface (in other words, z equals the maximum of the surface plus one). The particle is allowed to continue ''bouncing'' off the surface until it etches the surface or heads away from the surface. Finally, another particle is introduced and the whole process is repeated.

Determining how the particle is reemitted requires the surface normal to be known. There are many ways of defining the surface normal (since our surface is discrete), but we have found that the method used makes little difference as far as the scaling behavior is concerned. One way is to think of the surface as being made up of blocks and to use the normal of the surface of the block. We call this microscopic reemission. Since this is not very realistic, one should actually coarse-grain the surface and then compute the normal based on the coarse-graining. In practice, we used very small grains (containing only the block in question and its eight closest in-plane neighbors), because this shortens the crossover times, making it easier to see the scaling behavior. For the coarse-graining method, the x component of the slope at point (i,j) was taken to be $[h(i+1,j)+h(i+1,j-1)+h(i+1,j+1)-h(i-1,j)-h(i-1,j-1)-h(i-1,j+1)]/6$.

The Monte Carlo simulation has the advantage of being faster than integrating the continuum equation. Figure 6 shows the resulting surfaces for a 1024×1024 simulation of etching with nondirectional incoming flux, thermal reemission, and $s_0=0.05$, $s_1=1.0$ (this can take from four to eight days on a 300-MHz personal computer). The morphologies are similar to those of the continuum model shown in Fig. 3. The surfaces are made up of holes that grow with time. The height-height correlation functions for different times are shown in Fig. 7. The roughness exponent α, which is half the slope of the log-log plot of $H(r)$ for small r, increases with time and the latest time gives $\alpha=0.81$.

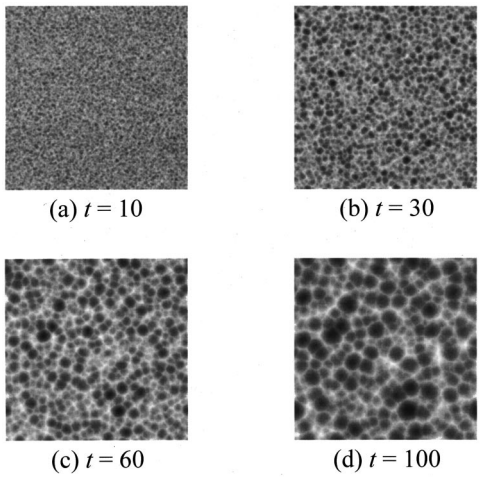

FIG. 6. Surface images for various times for a 1024×1024 Monte Carlo simulation with nondirectional flux and thermal reemission. (a) $t=10$, (b) $t=30$, (c) $t=60$, and (d) $t=100$. The gray scale is adjusted so that the highest point on the surface is white and the lowest point on the surface is black.

We also looked at the behavior of the model with different reemission modes and different incoming fluxes. The thermal and uniform reemission simulations with nondirectional flux both used microscopic reemission, while the specular reemission simulation with nondirectional flux and the thermal reemission simulation with directional flux were coarse-grained. The resulting surface images for different reemission modes and incoming fluxes are shown in Fig. 8. The morphology consists of holes in each case, but there are still slight differences in morphology. In particular, in the uniform distribution simulation, the hole depth varies more than it does in the other simulations. In Figs. 9, 10, and 11, we plot the interface width w, the correlation length ξ, and the average hole separation distance λ as functions of time for each simulation, respectively. The results show that, except for very early times, w and ξ are linearly dependent on time. A linear dependence also seems present in the plot of λ (with the possible exception of the uniform reemission simulation). In Fig. 12, we plot the roughness exponent α as a

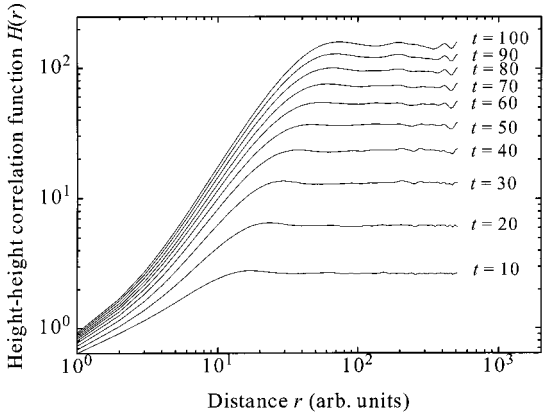

FIG. 7. Height-height correlation functions for various times for a 1024×1024 Monte Carlo simulation with nondirectional flux and thermal reemission.

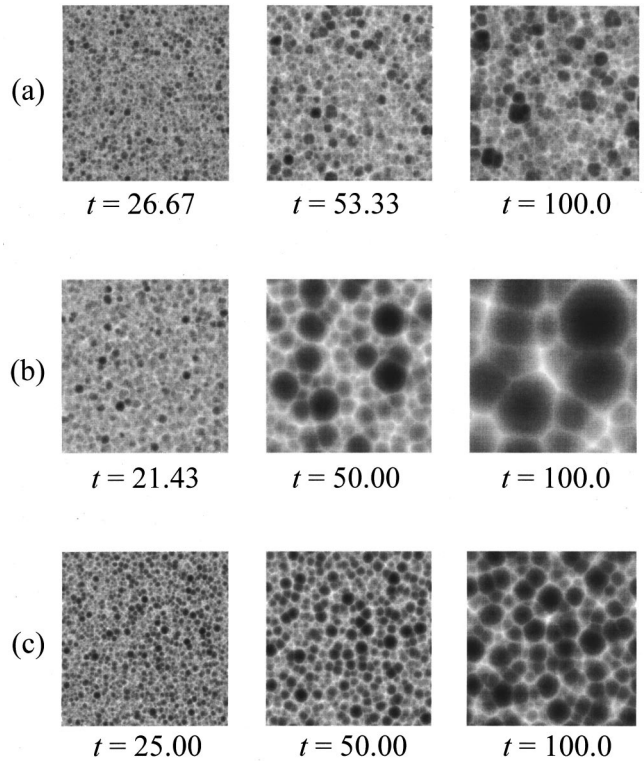

FIG. 8. Surface images for 1024×1024 Monte Carlo simulations at various times with (a) nondirectional flux and uniform reemission, (b) nondirectional flux and specular reemission, and (c) directional flux (from normal direction) and thermal reemission. The gray scale is adjusted so that the highest point on the surface is white and the lowest point on the surface is black.

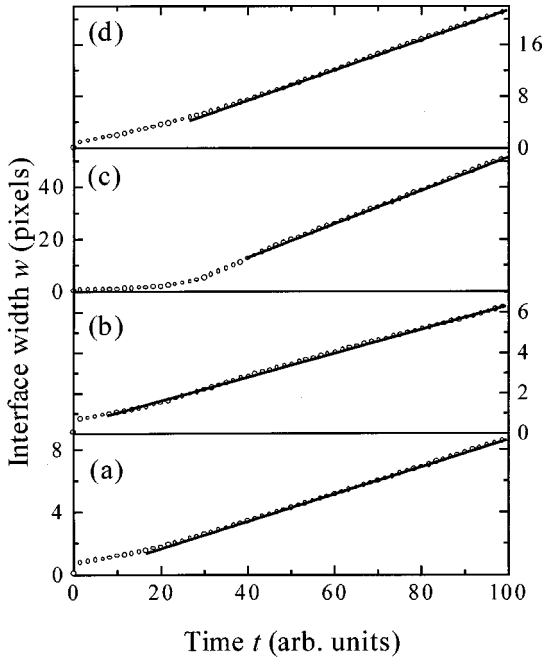

FIG. 9. Interface width w vs time for 1024×1024 Monte Carlo simulations with (a) nondirectional flux and thermal reemission, (b) nondirectional flux and uniform reemission, (c) nondirectional flux and specular reemission, and (d) directional flux (from normal direction) and thermal reemission. The good straight line fit to each plot in linear scale indicates that $\beta \approx 1$.

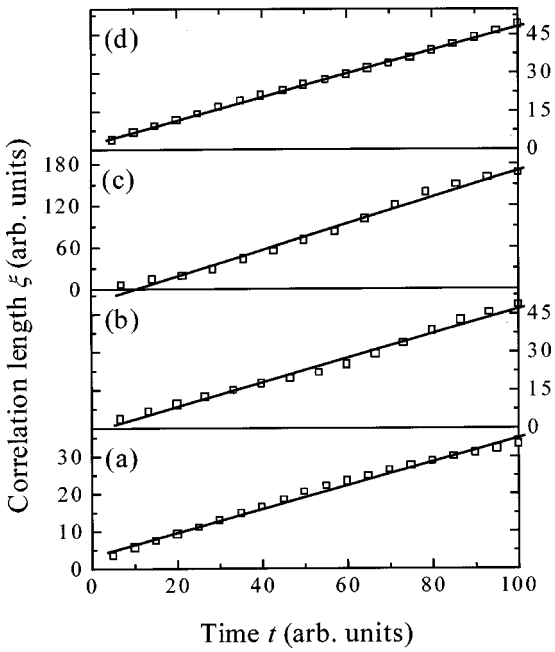

FIG. 10. Correlation length ξ vs time for 1024×1024 Monte Carlo simulations with (a) nondirectional flux and thermal reemission, (b) nondirectional flux and uniform reemission, (c) nondirectional flux and specular reemission, and (d) directional flux (from normal direction) and thermal reemission. The good straight line fit to each plot in linear scale indicates that $1/z \approx 1$.

function of time. We can see that, in each case, α is increasing towards some value. Although, in each case, w and ξ eventually have a linear dependence on time, the way in which the crossover occurs depends on the details of the model. Initially, in each case, there is noise regime in which $\beta \approx 0.5$. For the simulation with directional flux, the linear regime immediately follows. However, the simulations with nondirectional flux have a short shadowing regime, immediately after the noise regime, that precedes the linear regime.

IV. DISCUSSION

A. Universality

The Monte Carlo simulations that we have performed indicate a linear dependence of w and ξ on time for plasma-etching processes satisfying the first-order reemission approximation for all but one of the specific cases that we tried. Furthermore, the roughness exponent seems to be increasing towards a steady value. While it is difficult to see what the asymptotic value of α is, the value should be close to unity in each case. The simulation with uniform reemission shows the smallest roughness exponent, but its interface width has grown the least of all four simulations. Therefore it should take much longer for the noise (which is inherent in the Monte Carlo simulation) to become unimportant. Hence, the roughness exponent is lowered by the presence of noise for early times, but it should eventually become close to unity. These findings seem consistent with the existence of a new universality class, and in Table I, we list, along with our results, some popular growth and etching models and their associated scaling exponents. Note that we do not include other models such as the nonlinear MBE model of Lai and Das Sarma.[17]

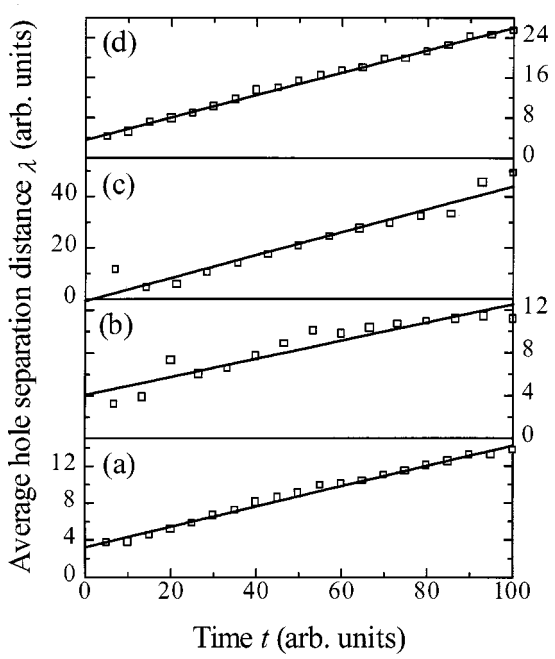

FIG. 11. Average hole separation λ versus time for 1024 ×1024 Monte Carlo simulations with (a) nondirectional flux and thermal reemission, (b) nondirectional flux and uniform reemission, (c) nondirectional flux and specular reemission, and (d) directional flux (from normal direction) and thermal reemission. The reasonable straight line fit to each plot in linear scale indicates that $\gamma \approx 1$.

The results of our simulations agree reasonably well with those of our plasma etching experiment.[8] In the experiment, we find that $\alpha = 0.96 \pm 0.06$, $\beta = 0.91 \pm 0.03$, and $z = 1.05 \pm 0.09$. We also find that the surface consists of holes that become larger with time. Some discrepancy exists between the numerical values of the growth exponents, but smoothening mechanisms could account for the slightly lower growth exponent in the experiment. Other mechanisms, such as the Schwoebel barrier effect or Kardar-Parisi-Zhang (KPZ) growth, cannot account for the observed experimental behavior since they predict growth exponents much less than unity. Our results are also compared to the plasma etching experiment of Brault, Dumas, and Salvan,[6] who show $\beta \approx 1$ and $z \approx 1.5$. In the experiment of Ref. 6, the ion/neutral ratio is higher than in conventional plasma etching. Hence, the incoming flux should be directional. Our simulations show that this should not affect the exponents, because the simulation with directional flux gives the same exponents as the simulations with nondirectional flux. However, we have not discussed the case of directional flux and specular reemission, which could exist for extremely high ion/neutral ratios (high-density plasma etching). This case is fundamentally different from the other cases, because the reemission direction is completely deterministic. In the case of directional (or nondirectional) flux and diffuse reemission, the reemission direction is explicitly random (following a certain probability distribution). In the case of nondirectional flux and specular reemission, the reemission direction is completely determined by the incoming direction, but the incoming direction is, itself, random. For directional flux with specular reemission, the incoming direction is always straight down, and the reemission direction is determined by the incoming direction and the surface normal. We found that, in this case, very large slopes tend to develop, which is consistent with the anisotropic nature of high-density plasma etching. We found a regime in which w is linear in t. However, we could not simulate longer times due to the large slopes that were generated. To prevent this, a smoothing mechanism would be required.

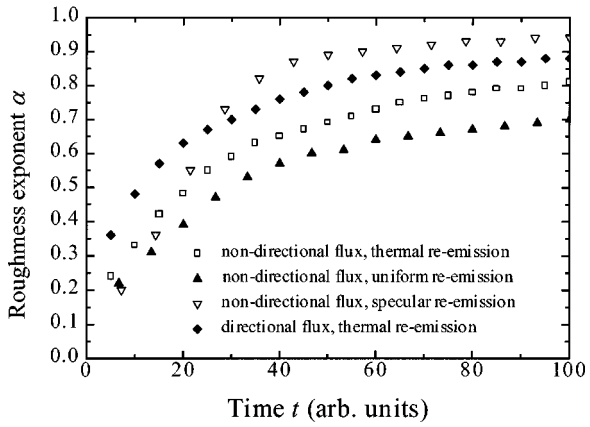

FIG. 12. Roughness exponent α vs time for 1024×1024 Monte Carlo simulations with nondirectional flux and thermal reemission, nondirectional flux and uniform reemission, nondirectional flux and specular reemission, and directional flux (from normal direction) and thermal reemission.

B. Local and nonlocal models

In general, there are two different kinds of growth/etching models: local and nonlocal. For local models, such as random deposition,[16] the Edwards-Wilkinson (EW) model,[18] the KPZ model,[15] or the Mullins diffusion model,[16,19] the growth/etching rate depends on the local properties of the interface. A general feature of such models is that $\partial h/\partial t$, at a given point, depends only on h or its derivatives, at that point. Hence, local models are described by differential equations. From Table I, we can see that these models usually give a growth exponent $\beta \leqslant 0.5$. This is because most local effects are smoothing effects. For ion bombardment, the ion erosion rate is proportional to the energy that incoming ions transfer to that particular surface point. The total energy transferred to a given point comes from all of the incoming ions surrounding that point, resulting in a Kuramoto-Sivashinsky (KS)-type equation.[20] However, in this case, though the energy-transfer process can cause instability in growth, it can be balanced by other smoothening mechanisms such as surface diffusion and the KPZ-type term. Therefore the overall behavior of the KS equation is stable.

For nonlocal models, the growth/etching rate depends not only on the local properties of the interface, but also on the surrounding environment; different conditions give very different behaviors. Nonlocal effects always require an integral over the surrounding surface. Therefore they can usually be expressed as integral-differential equations, making them much harder to study, both analytically and numerically, than local models. For example, if the shadowing effect is present in a deposition model, peaks of the film will receive more atoms, since the atoms strike the substrate from random angles. Meanwhile, valleys of the film surface will be

TABLE I. The predicted scaling exponents for several different $(2+1)$-dimensional growth and etching models. For comparison, experimental results are also included.

Model	α	β	z	Reference
Random deposition	Not defined	0.5	Not defined	1
Edwards-Wilkinson	0	0	2	1
KPZ	0.38	0.24	1.58	15
Mullins diffusion	1	0.25	4	16
KS (early time)	0.75–0.80	0.22–0.25	3.0–4.0	20
KS (late time)	0.25–0.28	0.16–0.21		20
Shadowing growth	Not available	1	Not available	7
Plasma reemission etching	~ 1	~ 1	~ 1	This work
Plasma etching experiment of Zhao *et al.*	0.96 ± 0.06	0.91 ± 0.03	1.05 ± 0.09	8
Plasma etching experiment of Brault, Dumas, and Salvan	Not available	1	1.5	6

deprived of incoming atoms because they are screened or shadowed by the peaks; hence they grow slower than the peaks. This may lead to an instability ($\beta=1$).[7] The plasma etching model we have proposed here is also a nonlocal model. The overall redistributed flux at each point depends on the surroundings and is expressed by the integral equation, Eq. (4). Under the assumption that the redistributed flux plays the major role in the etching, the valleys of the surface will receive more flux than the peaks, which causes an instability.

The exponents of our model make it easily distinguishable from other universality classes such as the KPZ or EW universality classes. Deposition with shadowing, though, gives $\beta=1$, just like our model. However, shadowing gives $\beta=1$ only for growth while first-order reemission gives $\beta=1$ only for etching, as we will discuss later.

C. Etching and growth processes

It is a common belief that etching is the reverse process of growth. Will the growth exponent β_e, for etching processes, differ from the growth exponent β_g, for growth processes, if the same mechanism works for both of them? Let us look at the local models first. For random deposition, atoms come down randomly either depositing on the surface or etching the surface. Clearly, in this case, the etching and growth equations are exactly the same. Therefore, $\beta_e=\beta_g=0.5$. For the EW model, the smoothing effect is due to the local thermal equilibrium of condensation and evaporation. For the Mullins diffusion model, the surface diffusion terms for both etching and growth are the same. Therefore in these two models $\beta_e=\beta_g$. We can also show that $\beta_e=\beta_g$ for the KPZ model. For the etching process, $\lambda_e=-\lambda$; therefore the etching process of KPZ type becomes

$$\frac{\partial h}{\partial t}=\nu\nabla^2 h-\frac{\lambda}{2}(\nabla h)^2+\eta(\mathbf{r},t). \tag{11}$$

If we make the transformation $h\rightarrow -h'$, then the etching KPZ equation can be rewritten as

$$\frac{\partial h'}{\partial t}=\nu\nabla^2 h'+\frac{\lambda}{2}(\nabla h')^2-\eta(\mathbf{r},t). \tag{12}$$

Since the noise is symmetric, we can replace $-\eta(\mathbf{r},t)$ with $\eta(\mathbf{r},t)$. The above equation then becomes

$$\frac{\partial h'}{\partial t}=\nu\nabla^2 h'+\frac{\lambda}{2}(\nabla h')^2+\eta(\mathbf{r},t). \tag{13}$$

This is the exact form of the KPZ growth equation, except that $h'=-h$. Therefore the growth exponent and etching exponent should be equal.

Now let us discuss the nonlocal models. For the shadowing effect, growth gives $\beta_g=1$. If we use the same effect to describe etching, as we discussed in the Introduction, the peaks of the surface will have a faster etching rate than the valleys, and therefore the unstable shadowing effect for growth becomes stable for etching (it is a smoothing effect), and $\beta_e\approx 0.02$.[21] For plasma etching, our reemission model predicts an instability that gives $\beta_e=1$. The reverse of this process could be a chemical vapor deposition process, and the reemission would tend to smoothen the surface. In this case, we have $\beta_g=0$. Details will be discussed elsewhere.[22]

The growth and etching exponents for the models we have discussed are shown in Table II. From the above-noted discussion we can conclude that, for the local models we have discussed above, the growth exponent β_g and the etching exponent β_e are equal. In those cases, growth and etch-

TABLE II. A comparison of the growth and etching exponents for several different $(2+1)$-dimensional models.

Model	Local/nonlocal	β_g	β_e
Random deposition	Local	0.5	0.5
Edwards-Wilkinson	Local	0	0
KPZ	Local	0.24	0.24
Mullins diffusion	Local	0.25	0.25
Shadowing growth	Nonlocal	1	0.02
Plasma reemission etching	Nonlocal	~ 0	~ 1

ing are identical. However, for the nonlocal models, the instability in either the growth or etching process will become stable in the reverse process.

D. Other considerations

In the present work, we have assumed that the reemitted flux has a higher sticking coefficient than the incident flux. This may happen since the reemitted flux has a slower velocity distribution than the incident flux. In the case of normally incident flux, however, this assumption is not necessary in order to generate the predicted rough etch fronts; the incident flux will simply act as noise, which will become unimportant for long enough etch times.

Another issue that should be considered is the etching rate. For each of the simulations, the time scale was normalized so that each simulation ends at $t=100$. However, one can measure time by the number of incoming particles that have hit the surface. In Fig. 13, we show the average height of the interface versus time (measured in the manner just mentioned). For each simulation, the last value on the graph corresponds to the $t=100$ point in the previous figures. One can see that, initially, the etching rate increases, but eventually becomes constant. The time it takes for the rate to become constant depends on the details of the model and is the longest for the specular reemission simulation; it takes about a third of the total simulation time for the rate to become constant. Initially, the rate is slow, because the surface starts out flat; hence, most particles are reemitted and head away from the surface. Later on, though, more reemitted particles hit the surface again, instead of heading away from it. The behavior of the etching rate also reflects the crossover behavior of the model; the interface width tends to crossover to linear behavior at about the same time that the etching rate becomes constant.

V. CONCLUSION

Our simulations support the conclusion that the etching of surface by first-order flux belongs to a new universality class

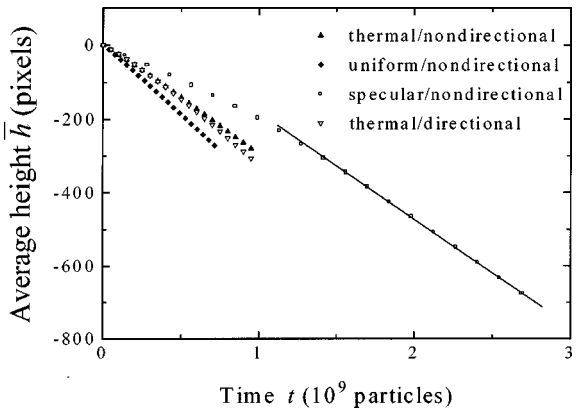

FIG. 13. Average interface height $\bar{h}$ vs time for 1024×1024 Monte Carlo simulations with nondirectional flux and thermal reemission, nondirectional flux and uniform reemission, nondirectional flux and specular reemission, and directional flux (from normal direction) and thermal reemission. Here, time is measured by the number of incoming particles that have hit the surface. The slope of each curve is equal to the etching rate.

with scaling exponents $\alpha\approx\beta\approx z\approx 1$, and this model can explain the results of plasma etching experiments in which scaling behavior was observed. Many other variations of this model exist, corresponding to different experimental systems. Obviously, the behavior will be different for growth processes (chemical vapor deposition, for example), and one would expect that $\beta<0.5$.

We should emphasize that the present work concentrates only on the scaling behavior of the plasma-etching front. A more practical issue is how to predict the actual roughness in microelectronics fabrication processes. According to Eq. (1), one has to know the details about the etchant flux such as the energy distribution, the momentum distribution, the sticking coefficients, and the noise amplitude. These are not trivial parameters in plasma etching. Also, as we have already mentioned in the Introduction, plasma-etching processes may involve more complex mechanisms. Detailed experiments would be needed to determine the contribution from the details of each mechanism. Moreover, since plasma etching in microelectronic fabrication is a pattern transform process, the role of the mask (which may cause redeposition) cannot be neglected. We hope that our work will stimulate more detailed studies in this area.

ACKNOWLEDGMENTS

This work was supported by NSF. The authors thank Dr. T. Cale and Dr. J. Amar for valuable discussions and J. B. Wedding for reading the manuscript.

[1] A.-L. Barabási and H. E. Stanley, *Fractal Concepts in Surface Growth* (Cambridge University Press, Cambridge, England, 1995).

[2] *Dynamics of Fractal Surfaces*, edited by F. Family and T. Vicsek (World Scientific, Singapore, 1991).

[3] Robert J. Hoekstra, Mark J. Kushner, Valeriy Sukharev, and Phillipe Schoenborn, J. Vac. Sci. Technol. B **16**, 2102 (1998).

[4] Vivek K. Singh, Eric S. G. Shaqfeh, and James P. McVittie, J. Vac. Sci. Technol. B **12**, 2952 (1994).

[5] Vivek K. Singh, Eric S. G. Shaqfeh, and James P. McVittie, J.

Vac. Sci. Technol. B **10**, 1091 (1992).
[6] Pascal Brault, Philippe Dumas, and Franck Salvan, J. Phys.: Condens. Matter **10**, L27 (1998); Richard Pétri, Pascal Brault, Olivier Vatel, Daniel Henry, Elie André, Philippe Dumas, and Franck Salvan, J. Appl. Phys. **75**, 7498 (1994).
[7] R. P. U. Karunasiri, R. Bruinsma, and K. Rudnick, Phys. Rev. Lett. **62**, 788 (1989); Jian Hua Yao and Hong Guo, Phys. Rev. E **47**, 1007 (1993); Christopher Roland and Hong Guo, Phys. Rev. Lett. **66**, 2104 (1991); G. S. Bales and A. Zangwill, *ibid.* **63**, 692 (1989).
[8] Y.-P. Zhao, Jason T. Drotar, G.-C. Wang, and T.-M. Lu, Phys. Rev. Lett. **82**, 4882 (1999).
[9] G. S. Oehrlein, P. J. Matsuo, M. F. Doemling, N. K. Rueger, B. E. E. Kastenmeier, M. Schaepkens, T. Standaert, and J. J. Beulens, Plasma Sources Sci. Technol. **5**, 1193 (1996); J. H. Keller, *ibid.* **5**, 166 (1996).
[10] G. S. Hwang, C. M. Anderson, M. J. Gordon, T. A. Moore, T. K. Minton, and K. P. Giapis, Phys. Rev. Lett. **77**, 3049 (1996).
[11] G. N. Patterson, *Molecular Flow of Gases* (Wiley, New York, 1956).
[12] G. N. Patterson, *Introduction to the Kinetic Theory of Gas Flow* (University of Toronto Press, Toronto, 1971).
[13] F. O. Goodman and H. Y. Wachman, *Dynamics of Gas-Surface Scattering* (Academic Press, New York, 1976).
[14] F. Family and T. Vicsek, J. Phys. A **18**, L75 (1985); F. Family, Physica A **168**, 561 (1990).
[15] M. Kardar, G. Parisi, and Y.-C. Zhang, Phys. Rev. Lett. **56**, 889 (1986); J. G. Amar and F. Family, Phys. Rev. A **41**, 3399 (1990); K. Moser, D. E. Wolf, and J. Kertész, Physica A **178**, 215 (1991).
[16] F. Family, J. Phys. A **19**, L441 (1986); Jacques G. Amar, Pui-Man Lam, and Fereydoon Family, Phys. Rev. E **47**, 3242 (1993).
[17] Z.-W. Lai and S. Das Sarma, Phys. Rev. Lett. **66**, 2348 (1991).
[18] S. F. Edwards and D. R. Wilkinson, Proc. R. Soc. London, Ser. A **381**, 17 (1982).
[19] W. W. Mullins, J. Appl. Phys. **28**, 333 (1957).
[20] Jason T. Drotar, Y.-P. Zhao, T.-M. Lu, and G.-C. Wang, Phys. Rev. E **59**, 177 (1999).
[21] Jason T. Drotar, Y.-P. Zhao, T.-M. Lu, and G.-C. Wang, Phys. Rev. B (to be published).
[22] Jason T. Drotar, Y.-P. Zhao, T.-M. Lu, and G.-C. Wang (unpublished).